

A Dual-Readout Method for Biothiols Detection Based on the NSET of Nitrogen-Doped Carbon Quantum Dots–Au Nanoparticles System

Xin Fu¹ · Danyu Gu¹ · Shengdong Zhao¹ · Ningtao Zhou¹ · He Zhang¹

Received: 16 January 2017 / Accepted: 4 April 2017 / Published online: 11 April 2017
© Springer Science+Business Media New York 2017

Abstract In this paper, a rapid, simple and highly sensitive method with dual-readout (colorimetric and fluorometric) based on the nanometal surface energy transfer (NSET) between nitrogen-doped carbon quantum dots (NCQDs) and gold nanoparticles (AuNPs) for detection of biothiols is described. Highly luminescent NCQDs were prepared via a simple one-step hydrothermal method by applying sucrose and glycine as carbon and nitrogen sources. The results showed the obtained NCQDs had an average particle diameter of 5 nm and highly luminescent. The maximum emission wavelength was 438 nm with an excitation wavelength of 360 nm. In this system, NCQDs and AuNPs were respectively treated as energy donors and energy acceptors, which enable the nanometal surface energy transfer (NSET) from the NCQDs to the AuNPs, quenching the fluorescence. However, biothiols was used as a competitor in the NSET by the strongly Au-S bonding to release NCQDs from the Au surface, which subsequently produces fluorescent signal recovery and the red-to-purple color change quickly. This probe showed rapid response, high selectivity and sensitivity for biothiols with dual colorimetric and fluorescent turn-on signal changes. The low detection limit was calculated as 20 nM by using L-cysteine acted as target molecules. The method was also successfully applied to the determination of biothiols in human serum samples, and the results were satisfying.

Keywords Biothiols · Nanometal surface energy transfer · Colorimetric · Fluorometric · Nitrogen-doped carbon quantum dots (NCQDs)

Introduction

Biological thiols (biothiols), such as glutathione (GSH), homocysteine (Hcy), and cysteine (Cys), plays a critical role in biological systems because of its wide distribution in living cells [1–3]. It has been noticed that abnormal levels of biothiols are linked to many diseases. Deficiency of cysteine is usually associated with a number of clinical situations, such as hair depigmentation, edema, skin damages, lethargy and loss of muscle and fat [1, 4, 5]. GSH usually serves as an antioxidant and protects cells from oxidative stress. Abnormal levels of GSH can lead to disturbance of physiological functions such as heart disease, stroke, and other neurological disorders. An elevated level of Hcy in human plasma is a risk factor for induce disorders including cardiovascular and Alzheimer's disease. Thus, pursuing an a sensitive, reliable, and convenient approach for trace analysis of biothiols is of great significance in biological, medical, and clinical studies and attract considerable interest in recent years. To date, many methods have been established for the determination of biothiols, such as electrochemistry [6], high-performance liquid/gas chromatography [7, 8], mass spectroscopy [9] and capillary electrophoresis [10]. Although some of these methods have more selective and sensitive, some inherent issues still cannot be avoided, such as expensive biomolecular reagents, complicated pretreatment of samples, or/and skilled operators. Up to now, more and more attentions have been paid to develop novel fluorescent method for rapid, technically simple, and efficient detection of biothiols without any expensive apparatus [11–14].

✉ He Zhang
mzhang_he@126.com

Xin Fu
fuxin1129@126.com

¹ School of Chemistry and Chemical Engineering, Hunan Institute of Engineering, Xiangtan 411104, China

Nanometal surface energy transfer (NSET) is a kind of energy transferring from an energy donor to an acceptor (AuNPs) through nonradioactive dipole–dipole coupling. Compared to fluorescence resonance energy transfer (FRET), NSET has a higher energy transfer rate from the organic donor to the AuNPs acceptor and a longer quenching distance. So it has been widely used in various research areas [15–17].

Carbon quantum dots (CQDs) as new carbon nanomaterials were ideal fluorophores, and recently attract considerable attention. Compared with conventional heavy metal (e.g., Hg, Cd, Pb) -based inorganic semiconductor QDs and organic dye, CQDs with higher photostability and lower toxicity have shown excellent performances in bio-applications [18–20], especially in development of biosensors. Until now, many methods have been utilized for the preparation of CQDs, such as electrochemical exfoliation [21, 22], thermal decomposition or oxidation [23, 24], laser ablation [25], thermal dehydration [26], and microwave irradiation [27]. Nevertheless, most methods are not ideal for practical applications because of their low quantum yields, expensive equipment and/or intricate processes. Thus, it is of great significance through surface modification to achieve high fluorescence efficiency of CQDs.

In the present work, the highly luminescent nitrogen-doped quantum dots (NCQDs) was prepared by a facile one-pot hydrothermal route using sucrose and glycine as carbon and nitrogen sources. We designed a highly sensitive, simple and naked-eye method using as-prepared NCQDs for dual read-outs (colorimetric and fluorometric) detection of the low level of biothiols based on NSET technique. The dual-readout assay combining colorimetric characteristics of AuNPs with fluorometric sensitive measurement of NSET can be used to visually detect trace amounts of biothiols. Moreover, this method shows rapid response, cost-effective, much better sensitivity and can thereby be a reliable option to determine the concentration of biothiols in real samples.

Experimental

Materials and Instruments

Sucrose, glycine, trisodium citrate dehydrate(98%), chloroauric acid ($\text{HAuCl}_4 \cdot 3\text{H}_2\text{O}$), and L-cysteine (98%) were purchased from Sigma-Aldrich Chemical Co. All chemicals and solvents were obtained from the commercial sources and used directly without further purification. Ultrapure water used was purified using a Millipore filtration system (NANOPure, USA) with a resistivity of 18.0 $\text{M}\Omega$ cm. All glassware used in this preparation was thoroughly cleaned in aqua regia (three parts HCl, one part HNO_3), rinsed in doubly distilled water, and oven-dried prior to use.

Morphology of the synthesized nanoparticles was examined by a SU3500 scanning electron microscope (Hitachi, Japan). Absorption spectra were obtained by a UV-1800 UV-vis spectrophotometer (Shimadzu, Japan) using a quartz cell with the path length of 1.0 cm. Fluorescence spectra were performed with a LS-55 fluorescence spectrophotometer (PerkinElmer, USA) with a 1.0 cm quartz cell with 10 nm band width for both the excitation and emission monochromators. The pH was measured using a PHS-25 pH meter (Shanghai, China). All optical measurements were carried out at room temperature under ambient conditions.

Preparation of Citrate-Stabilized AuNPs

Citrate-stabilized AuNPs were prepared following the modified Frens' method [28]. Firstly, 2 mL of 1% aqueous solution of HAuCl_4 in 48 mL of water was heated to boil with vigorous stirring, and 5 mL of 1% trisodium citrate was added quickly. The solution turned deep blue within 20 s and the final color change to deep-red. The solution was then heated for an additional 10 min. The solution was cooled to room temperature and stored at 4 °C.

Preparation of Nitrogen-Doped Carbon Quantum Dots (NCQDs)

NCQDs were prepared by one-step hydrothermal treatment using sucrose and glycine as both carbon and nitrogen sources. Briefly, sucrose (2.0 g) and glycine (1.0 g) were mixed with Nanopure water (25 mL) by ultrasonication. The solution was transferred to a Teflon-equipped stainless-steel autoclave and heated hydrothermally at 180 °C for 8 h. After cooling to room temperature, the brown-yellow product was centrifuged at a high speed (10,000 rpm) for 15 min. Then, the supernatant was dialyzed against pure water through a dialysis membrane (MWCO of 1000) for 1 day and the obtained supernatant was vacuum-dried to collect NCQDs.

Quantum Yield Measurement

The quantum yield (QY) of the as-prepared NCQDs was measured according to a literature procedure [29] by using quinine sulfate in 0.1 M H_2SO_4 (literature quantum yield 0.54 at 360 nm) as a standard. Absolute values are calculated using the standard reference sample that has a fixed and known fluorescence quantum yield value. The quantum yield of the NCQDs was determined at the excitation wavelength of 360 nm by the following equation:

$$\phi_x = \phi_{st} \frac{F_x A_{st} \eta_x^2}{F_{st} A_x \eta_{st}^2}$$

where Φ is quantum yield, F is the measured integrated emission intensity, η is the refractive index of the solvent, and A is the optical density. The subscript “st” refers to the referenced fluorophore (quinine sulfate in 0.1 M H_2SO_4) with known quantum yield and “x” refers as the samples for the determination of quantum yield.

Preparation of the NSET System

The NCQDs-AuNPs NSET system was prepared at room temperature in PBS buffer (pH 8.0) [30]. Briefly, a 200 μL stock solution of NCQDs ($0.5 \text{ mg}\cdot\text{mL}^{-1}$) and PBS buffer solution (1.5 mL) were added with stirring into solutions of the as-prepared citrate-AuNPs (10 nM, 1.0 mL) in a centrifuge tube, and then diluted to 5.0 mL with deionized water. After 20 min reaction, the fluorescence spectra were measured at room temperature with excitation at 360 nm.

Detection Procedure of Cys

A 0.1 M stock solution of L-cysteine was prepared in PBS buffer solution (pH = 7.0), from which various cysteine concentrations were prepared by serial dilution. Different concentrations of L-cysteine (200 μL) were mixed with a solution of NCQDs-AuNPs (2 mL) and B-R buffer solution (500 μL), then the mixture was diluted to 5.0 mL with water and kept in the dark for 20 min. The UV-vis absorption and fluorescence were measured respectively. The procedures for all the optimization and control experiments are the same as described above.

The detection of urine sample: The urine sample (1.0 mL) was diluted by acetonitrile (1.0 mL) for removing the interference of proteins and other substances in urine, respectively [31]. After standing for 10 min to precipitate proteins, the sample was centrifuged for 10 min at 12000 rpm at 20 °C. The supernatant was dried by vacuum at 50 °C for 12 h, and then 100.0 μL Tris-HAc buffer was added to re-dissolve sample and stored at 4 °C until fluorescence analysis.

Results and Discussion

Characterization of AuNPs and NCQDs

The optical properties of the as-prepared NCQDs were examined by UV-vis absorption spectra and fluorescence spectra (Fig. 1a). It could be seen that the prepared NCQDs solution shows an absorption peak centered at 283 nm and a strong PL emission spectrum centered at 438 nm when it is excited at 360 nm. The bright blue fluorescence emitted from NCQDs could be seen under UV light (inset of Fig. 1a). The quantum yields (QY) was obtained to be 9.8% with quinine sulfate as the reference. When excitation wavelengths was changed in the range of 340–420 nm in 10 nm increments, the emission peak

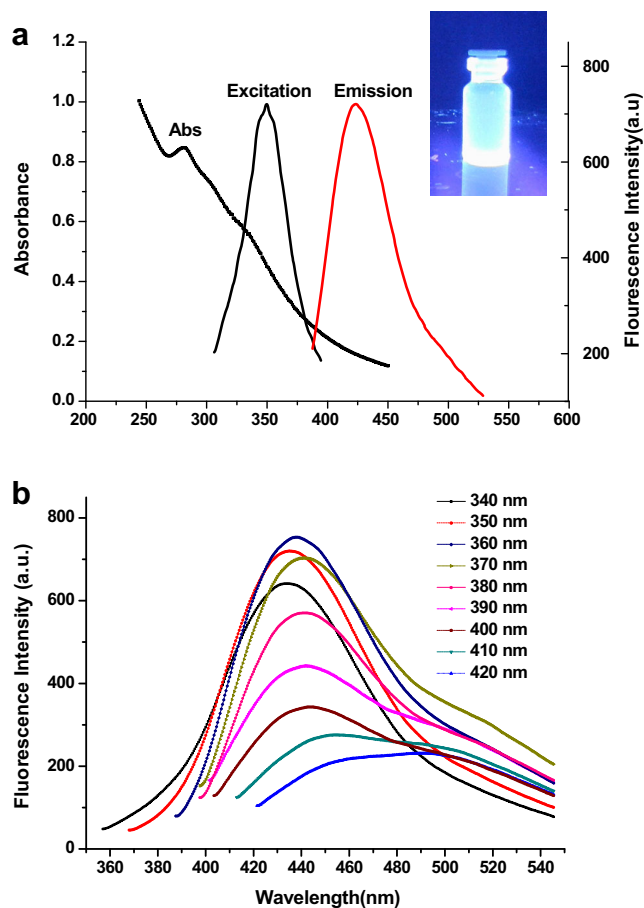


Fig. 1 UV-Vis absorption and fluorescence spectra of the NCQDs in aqueous solutions (a). Inset shows images of the obtained NCQDs under UV light. Fluorescence spectra of the NCQDs at excitation wavelengths from 340 nm to 420 nm in 10 nm increment (b)

of the NCQDs shifts to longer wavelengths (Fig. 1b). The maximum fluorescence emission intensity can be obtained when it is excited at 360 nm. The emission shifts dependence of the excitation wavelength increases, indicating a distribution of the different surface energy traps of the as-prepared NCQDs [32].

The Fig. 2a showed the photostability of NCQDs nanocrystals that were compared against traditional fluorescence dye – FITC and Rhodamine B. The fluorescence intensity was measured every 10 min at respective optimal excitation wavelengths. The results proved that the NCQDs are more stable than fluorescence dye. The fluorescence signature of NCQDs was not obviously changed, while the fluorescence intensity of fluorescence dye was reduced about 80% within 15 min. The sizes of the Au nanoparticles were about 13 nm by TEM analysis. The SEM image of NCQDs also reveals that the nanocrystals are irregular spherical and the diameters were mainly distributed in the narrow range from 4 nm to 6 nm, with an average size of 5 nm (Fig. 2b and Fig. 2c). The functional groups on the surface of NCQDs were investigated using FTIR spectrometry (Fig. 2d). Bands at 3100–3500 cm^{-1} are characteristic absorption of O-H and N-H stretching vibration, respectively. Bands at

Fig. 2 Fluorescent photostability of NCQDs, FITC and Rhodamine B (a). Morphology of AuNPs (b) and NCQDs (c). FTIR spectra of NCQDs (d)

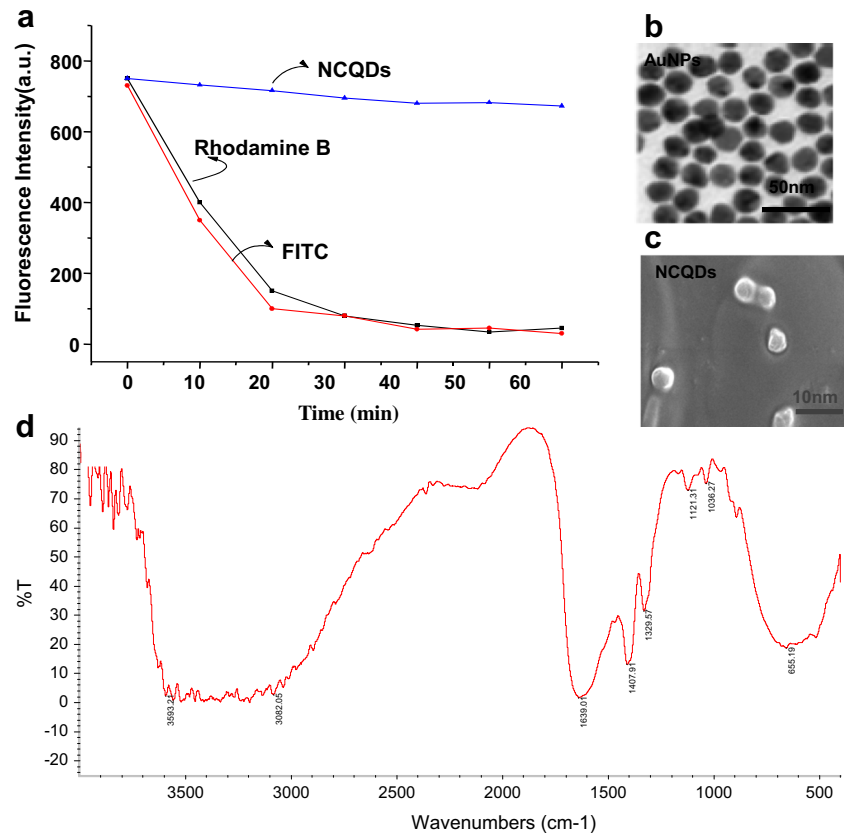
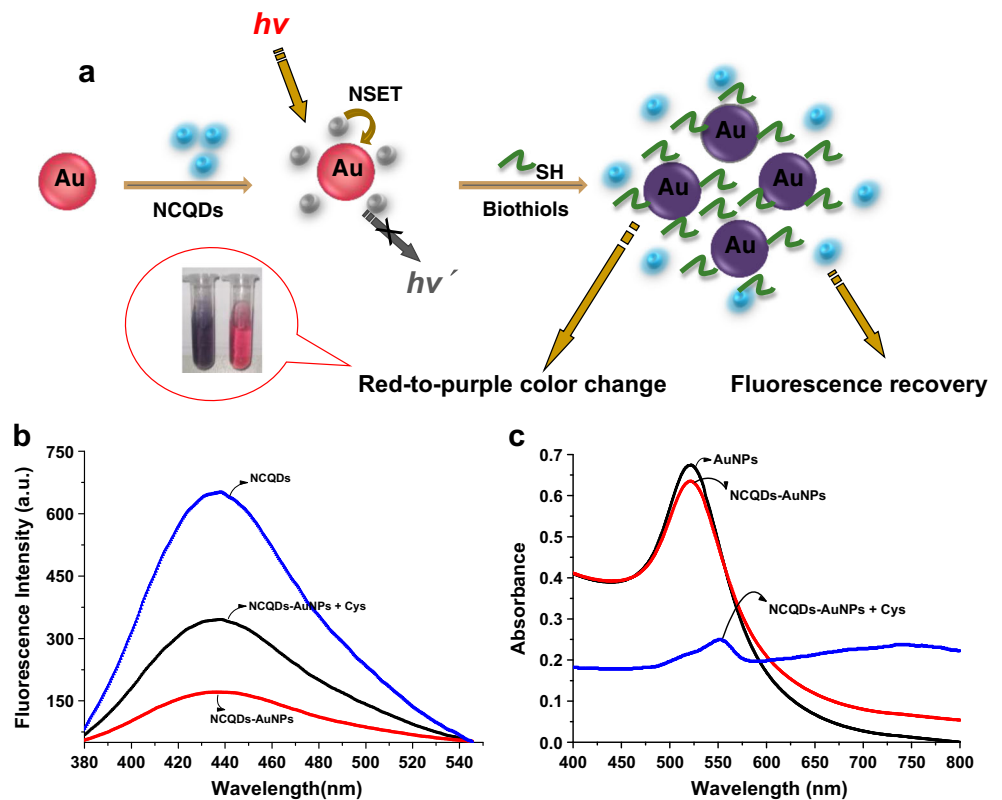


Fig. 3 Design of the dual-readout (colorimetric and fluorometric) assay for biothiols (a), fluorescence spectra of the system (b) and their corresponding UV-vis absorption (c)



1639 cm^{-1} is respectively assigned to stretching vibration of $\text{C}=\text{O}$ [33, 34] and $\text{C}-\text{N}$ [35, 36]. Bands at 1329 and 1407 cm^{-1} are ascribed to the typical stretching vibration modes of $\text{C}=\text{N}$ and $\text{C}-\text{N}$ heterocycles [37]. Bands at 1036 cm^{-1} is assigned to vibration of $\text{C}-\text{O}$ [38]. These results prove as-prepared carbon quantum dots are nitrogen-doped. The stable, monodisperse and highly fluorescent nanoparticles as fluorescent probes were studied as follows.

Mechanism of the Dual-Readout Assay for Biothiols

AuNPs have been widely used in the biosensor field because of the higher extinction coefficient and a broad absorption spectrum in a visible light. The absorption spectrum of AuNPs is overlapped with the emission wavelength of NCQDs which result in highly efficient energy transfer from the NCQDs to AuNPs. The designed assay principle is illustrated in Fig. 3a. In this system, NCQDs can be readily adsorbed onto surfaces of citrate-stabilized AuNPs via electrostatic interactions to result in highly efficient energy transfer from the NCQDs to AuNPs. Nevertheless, biothiols demonstrates stronger affinity towards AuNPs than NCQDs because of the $\text{Au}-\text{S}$ bonding, which renders the biothiols

molecule to encapsulate AuNPs in priority, thus removing NCQDs from the Au surface to recover the fluorescence of NCQDs. It also cause the red-to-purple color change in the process of anti-aggregation of AuNPs color change quickly in that aggregation of AuNPs, the aggregation state change of AuNPs induced by Cys can be visualized by the naked eye.

To verify the mechanism, we prepared NCQDs-AuNPs solution by allowing an optimized concentration. Herein, positively charged amino groups (NH_2^-) of NCQDs can be readily adsorbed on the surface of negatively charged citrate-AuNPs via electrostatic interaction. As a result, the fluorescence of NCQDs can be quenched by AuNPs through NSET (Fig. 3b). The fluorescence intensity of NCQDs -AuNPs system is proportional to the concentration of quencher (AuNPs) and quenching constant (K_{sv}) was calculated to be $0.92 \times 10^9\text{ L} \cdot \text{mol}^{-1}$ using the Stern-Volmer equation: $F_0/F = K_{\text{sv}} \times [Q] + 1$ (F and F_0 are the fluorescence intensities with and without the presence of the AuNPs respectively, $[Q]$ is the concentration of the quencher, K_{sv} is the quenching constant). Upon the addition of Cys into a NCQDs-AuNP solution, the $-\text{SH}$ of Cys can bind more strongly onto surfaces of AuNPs than NCQDs via specific $\text{Au}-\text{S}$ bonding, accompanied the release of NCQDs and the fluorescence was restored.

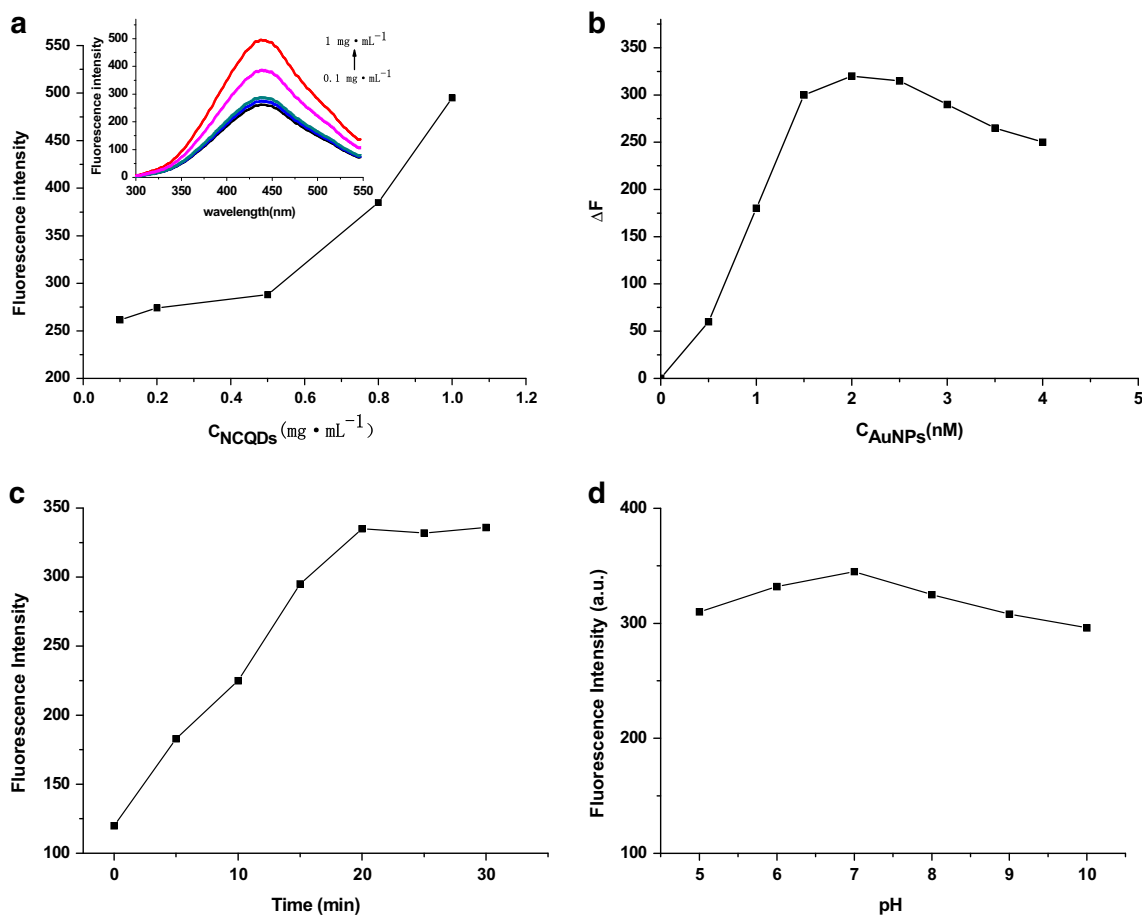


Fig. 4 Effect of concentration of NCQDs (a), concentration of AuNPs (b), reaction time (c) and pH(d) upon the fluorescence intensity of system

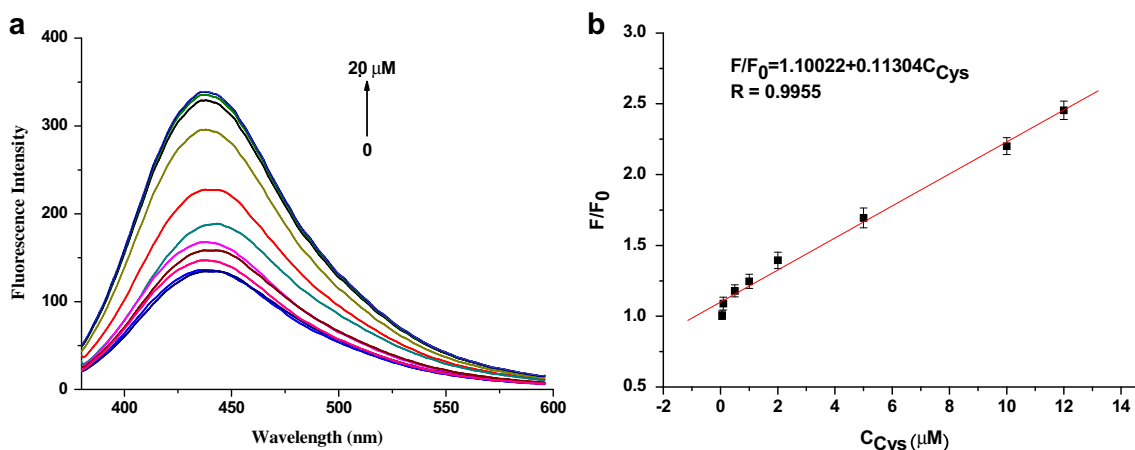


Fig. 5 FL restoration of the NCQDs-AuNPs system (a) and the linear calibration data (b) versus the concentration of Cys

Simultaneously, AuNPs color changed from red to purple, along with the increase of Cys concentration, $-SH$ that attached onto different AuNP surfaces are able to cause the aggregation of AuNPs (Fig. 3c). This method shows rapid response, cost-effective, high selectivity and sensitivity with dual colorimetric and fluorescent signal changes and can thereby be a reliable option to determine the concentration of biothiols in biological samples.

Effect of Concentration of NCQDs

The effect of concentration of NCQDs on the NSET system is studied (Fig. 4a). For each reaction, 200 μL stock solution of NCQDs with a concentration ranging from 0.1 to 1 $\text{mg}\cdot\text{mL}^{-1}$ and 1.5 mL PBS buffer solution was added with stirring into solutions of the 1.0 mL AuNPs (10 nM), and then diluted to 5.0 mL with deionized water. The fluorescence spectra of the NCQDs-AuNPs solutions were measured with excitation at 438 nm. It is obvious that NCQDs -AuNPs fluorescence was quite weak due to the efficient NSET and there was not obviously changed in fluorescence intensity when the concentration of NCQDs was below 0.5 $\text{mg}\cdot\text{mL}^{-1}$ (insert, Fig. 4a).

Nevertheless, the fluorescence response is boosted up with the concentration of N-CQDs over 0.5 $\text{mg}\cdot\text{mL}^{-1}$. This indicates that the excess NCQDs cannot contribute to the NSET between NCQDs and AuNPs, but increase the background value. So, the NCQDs concentration of 0.5 $\text{mg}\cdot\text{mL}^{-1}$ was selected for all of the experiments.

Effect of Concentration of AuNPs

Concentration of AuNPs has great effect on the performance of the probe system. We carried out reactions where all parameters were fixed with the exception of the final concentration AuNPs in a range from 1 nM to 5 nM. The fluorescence spectra of the NCQDs-AuNP solution were measured with excitation at 360 nm. As shown in Fig. 4b, there is a continuous significant increase of the ΔF ($F-F_0$, F_0 and F are the PL intensities of the NCQDs at 438 nm in the absence and presence of Cys) in the presence of Cys until the final concentration of AuNPs reached 2 nM. On the contrary, the fluorescence intensity was decreased when the final concentration was over 2 nM, indicating that NCQDs would have more opportunities to be closer to the excess amount AuNPs to cause quenching more thoroughly.

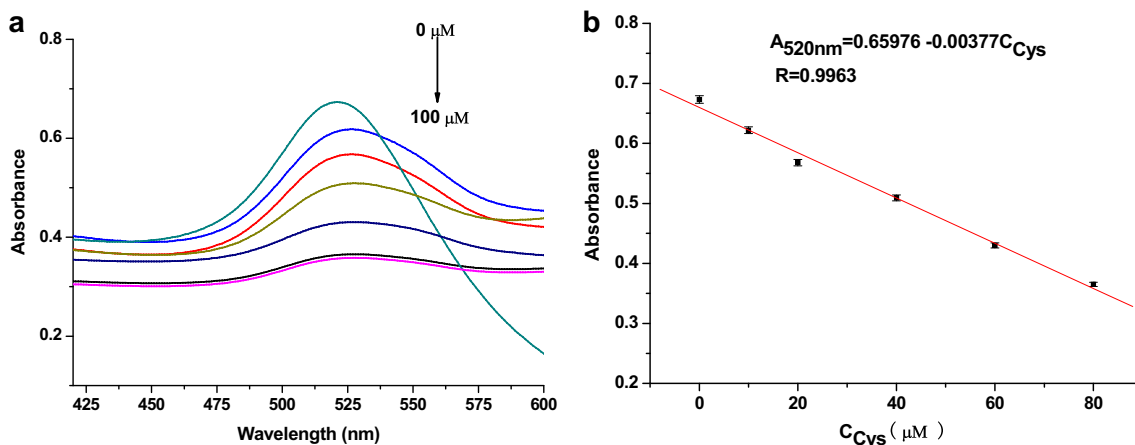


Fig. 6 The absorbance of the NCQDs-AuNPs system at 520 nm (a) the linear calibration data (b) versus the concentration of Cys

Table 1 Comparison of methods for the determination of biothiols

Detection method	Linear range	Detection limit	Reference
Colorimetry	10–100 μM	Not Given	[39]
Electrochemistry	1–400 μM	50 nM	[40]
Electrochemistry	0.3–3.6 μM, 3.9–7.2 μM	90 nM	[41]
Fluorimetry(FRET)	2–200 nM	Not Given	[38]
Fluorimetry(FRET)	5.0–50.0 μM	3.6 μM	[42]
Fluorimetry(FRET)	0–0.3 mM	Not Given	[43]
Fluorimetry(NSET)	0.025–4.5 μM	8.0 nM	[17]
Fluorimetry(NSET) and colorimetric	0–137 μM	98 nM	[44]
Fluorimetry(NSET) and colorimetric	0.05–12 μM	20 nM	Our work
	0–100 μM		

Effect of Reaction Time

The reaction rate of Au-S bonding is very quickly and the influence of reaction time was investigated. As shown in Fig. 4c, the fluorescence was enhanced with the reaction time between 10 and 20 min and the response started to level off above 20 min. This indicated that the interaction of NCQDs-AuNPs with L - cysteine had reached equilibrium after 20 min. Accordingly, 20 min was selected as the operating reaction time.

Effect of pH and Buffer

In addition, the fluorescent properties of pure NCQDs solution and the fluorescent detection are both related to the pH value of media. The effect of pH on the FL intensity was studied over the pH range from 5.0 to 9.5. It can be seen that the fluorescence response reaches the maximum at pH 7.0 (Fig. 4d). In addition, several buffer systems, such as carbonate buffer, phosphate-buffered saline, tris-buffered saline, britton-robinson (B-R) buffer solution, were tested. It was found that the best buffer system is phosphate-buffered saline (PBS). So 10 mmol/L PBS (pH = 7.0) was used as reaction buffer throughout.

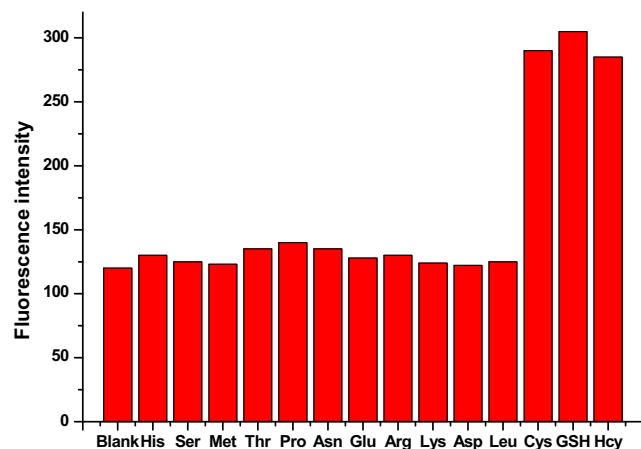


Fig. 7 Tests for the interference of coexisting substances

Analytical Performance

Under the optimum experimental conditions, the effect of L-cysteine on the NSET system had been investigated. As shown in Fig. 5a, the FL of the system would be recovered with increase of the concentration of Cys from 0 to 20 μM. The FL intensity ratio (F/F_0 , F_0 and F are the PL intensities of the NCQDs at 438 nm in the absence and presence of Cys) exhibits a linear response to Cys concentration in the range of 0.05–12 μM, the calibration curve can be expressed as $F/F_0 = 1.10022 + 0.11304C_{Cys}$ with the relative coefficient of 0.9955 (Fig. 5b). The limit of detection ($3\sigma/b$) for L - cysteine is 20 nM, where σ is the known standard deviation of ten measurements for the reagent blank’s signal and b is the slope of the calibration curve at low analyte concentration).

Moreover, the aggregation of AuNPs induced by Cys also can be quantitated by UV–vis spectroscopy. The increase of Cys concentration resulted in the systematic decrease of the absorbance at 520 nm, which is consistent with the color change of AuNPs suspension displayed in Fig. 3a. Figure 6 shows A_{520} values versus various concentrations of Cys, respectively. The absorbance signal at 520 nm gradually decreases with the Cys concentration from 10 to 120 μM (Fig. 6a), and the A_{520} decreased linearly from 0 to 100 μM using the equation $A_{520nm} = 0.65976 - 0.00377C_{Cys}$ with a linear correlation $R = 0.9963$ (Fig. 6b).

Table 1 shows the comparison of LOD and linear range with those of different methods for biothiol analysis. It is suggested that such NCQDs system as a fluorescent sensor

Table 2 Results of analysis of three human urine samples

sample	Biothiols in samples/(μM)	Concentration found (μM) ^a (mean ± SD)	Recovery ^a /%	RSD ^a /%
1	0.50	0.52 ± 0.02	104.0%	3.8%
2	2.20	2.26 ± 0.10	102.7%	4.4%
3	3.50	3.43 ± 0.14	98.0%	4.1%

^a denotes average of three determinations

exhibits superior sensitivity for biothiol analysis, wide linear response range and high possibility for the quantitative detection of biothiol analysis. Meanwhile, the proposed method can provide both fluorescence and colorimetric signals for the detection of thiols.

The Influences of Coexisting Substances

To verify the performance of our sensor for biothiol detection in practical applications, we investigated the effect of the other essential amino acids at a concentration of 10 μ M under the optimum experimental conditions. The experimental results are shown in Fig. 7. It is clear that only GSH/Cys/Hcy showed significantly higher fluorescence intensity and no apparent enhancement of fluorescence intensity for other amino acids compared to the blank. The results confirmed the mechanism that only -SH can be used as a competitor in the NSET to bind onto surfaces of AuNPs and recover the fluorescence of NCQDs.

Real Sample Determination

To prove the feasibility and practicality of the method, the present method is applied to directly detect total biothiols in the human urine samples. The results are listed in Table 2. The analytical results show that the values found from the three samples by this proposed method are identical with the Cysteine Assay Kit (Enzyme labelling method), and the recovery results ranged from 98.0% to 104.0% with a satisfied relative standard deviation (RSD 3.8%–4.4%) indicating that no significant interference for the biothiols determination in urine samples. Therefore, this proposed dual-readout assay for detecting biothiols is applicable.

Conclusions

The highly luminescent NCQDs were synthesized by a facile one-pot hydrothermal route and a simple and flexible method based on the NSET between NCQDs and AuNPs with dual-readout detection for biothiols is proposed. The dual-readout assay combining colorimetric characteristics of AuNPs with fluorometric sensitive measurement of NSET can be used to visually detect trace amounts of biothiols. Under the optimum conditions, when Cys acted as target molecules, it could be detected with high sensitivity and low detection limit down to 20 nM. Moreover, the sensors have been successfully employed for the detection of the total biothiols in human serum samples with satisfactory results. We expect such a NSET system between NCQDs and AuNPs has desirable applications in the analytical areas especially in the development of bio-sensing systems.

Acknowledgments The work is supported by Provincial Natural Science Foundation of Hunan (No. 2015JJ2039, No.14JJ3133), Scientific Research Fund of Hunan Provincial Education Department (16B060).

References

- Shahrokhian S (2001) Lead phthalocyanine as a selective carrier for preparation of a cysteine- selective electrode. *Anal Chem* 73:5972–5978
- Wang WH, Rusin O, Xu XY, Kim KK, Escobedo JO, Fakayode SO, Fletcher KA, Lowry M, Schowalter CM, Lawrence CM, Fronczek FR, Warner IM, Strongin RM (2005) Detection of homo-cysteine and cysteine. *J Am Chem Soc* 127:15949–15958
- Spataru N, Sarada BV, Popa E, Tryk DA, Fujishima A (2001) Voltammetric determination of L-cysteine at conductive diamond electrodes. *Anal Chem* 2001(73):514–519. doi:10.1021/ac000220v
- Fei SD, Chen JH, Yao SZ, Deng GH, He DL, Kuang YF (2005) Electrochemical behavior of l-cysteine and its detection at carbon nanotube electrode modified with platinum. *Anal Biochem* 339:29–35
- Shang L, Qin CJ, Wang T, Wang M, Wang LX, Dong SJ (2007) Fluorescent conjugated polymer-stabilized gold nanoparticles for sensitive and selective detection of cysteine. *J Phys Chem C* 111: 13414–13417
- Tseng KS, Chen LC, Ho KC (2006) Amperometric detection of cysteine at an In³⁺ stabilized indium hexacyanoferrate modified electrode. *Electroanalysis* 18:1306–1312
- Sawula W, Banecka-Majkutewicz Z, Kadziński L, Jakóbkiewicz-Banecka J, Wegrzyn G, Nyka W, Banecki B (2008) Improved HPLC method for total plasma homocysteine detection and quantification. *Acta Biochim Pol* 55:119–125
- Tcherkas YV, Kartsova LA, Krasnova IN (2001) Analysis of amino acids in human serum by isocratic reverse-phase high-performance liquid chromatography with electrochemical detection. *J Chromatogr A* 913:303–308
- Johnson JM, Strobel FH, Reed M, Pohl J, Jones DP (2008) A rapid LC-FTMS method for the analysis of cysteine, cystine and cysteine/cystine steady-state redox potential in human plasma. *Clin Chim Acta* 396:43–48
- Yu H, Xu L, You TY (2013) Indirect electrochemiluminescence detection of lysine and histidine separated by capillary electrophoresis based on charge displacement. *Luminescence* 28:217–221
- Yu LR, Li L, Ding YP, Lu YX (2016) A fluorescent switch sensor for glutathione detection based on Mn-doped CdTe quantum dots - methyl viologen nanohybrids. *J Fluoresc* 26:651–660
- Vimal K, Bhardwaj HS, Singh N (2014) Ratiometric fluorescent probe for biothiol in aqueous medium with fluorescent organic nanoparticles. *Talanta* 129:198–202
- Zhang QE, Deng T, Li JS, Xu WJ, Shen GL, Yu RQ (2015) Cyclodextrin supramolecular inclusion-enhanced pyrene excimer switching lifetime-resolved fluorescence detection of biothiols in serum. *Biosens Bioelectron* 68:253–258
- Zuo QP, Li B, Pei Q, Li ZJ, Liu SK (2010) A highly selective fluorescent probe for detection of biological samples thiol and its application in living cells. *J Fluoresc* 20:1307–1313
- Fu X, Liu Y, Wu ZT, Zhang H (2014) Highly sensitive and naked eye dual-readout method for L-cysteine detection based on the NSET of fluorophore functionalized gold nanoparticles. *Bull Kor Chem Soc* 35:1159–1164
- Hou J, Zhang FS, Yan X, Wang L, Yan J, Hong D, Ding L (2015) Sensitive detection of biothiols and histidine based on the recovered fluorescence of the carbon quantum dots–hg(II) system. *Anal Chim Acta* 859:72–78

17. Liu C, Wu T, Huang CZ (2010) Gold nanoparticles surface energy transfer and its application to highly selective and sensitive detection of cysteine. *Sci Sin Chim* 40:531–537
18. Saineelima B, Kasibabu B, D'souza SL, Jha S, Kailasa SK (2015) Imaging of bacterial and fungal cells using fluorescent carbon dots prepared from *Carica papaya* juice. *J Fluoresc* 25:803–810
19. Baker SN, Baker GA (2010) Luminescent carbon nanodots: emergent nanolights. *Angewandte Chemie-International Edition* 49:6726–6744
20. Shan XY, Chai LJ, Ma JJ, Qian ZS, Chen JR, Feng H (2014) B-doped carbon quantum dots as a sensitive fluorescence probe for hydrogen peroxide and glucose detection. *Analyst* 139:2322–2325
21. Li Y, Hu Y, Zhao Y, Shi G, Deng L, Hou Y, Qu L (2011) An electrochemical avenue to green-luminescent graphene quantum dots as potential electron-acceptors for photovoltaics. *Adv Mater* 23:776–780
22. Ananthanarayanan A, Wang X, Routh P, Sana B, Lim S, Kim DH, Lim KH, Li J, Chen P (2014) Facile synthesis of graphene quantum dots from 3D graphene and their application for Fe^{3+} sensing. *Adv Funct Mater* 24:3021–3026
23. Tian L, Ghosh D, Chen W, Pradhan S, Chang X, Chen S (2009) Nanosized carbon particles from natural gas soot. *Chem Mater* 21:2803–2809
24. Bourlinos AB, Stassinopoulos A, Anglos D, Zboril R, Georgakilas V, Giannelis EP (2008) Photoluminescent carbogenic dots. *Chem Mater* 20:4539–4541
25. Atienzar P, Primo A, Lavorato C, Molinari R, Garcia H (2013) Preparation of graphene quantum dots from Pyrolyzed alginate. *Langmuir* 29:6141–6146
26. Zhang B, Liu CY, Liu Y (2010) A novel one-step approach to synthesize fluorescent carbon nanoparticles. *Eur J Inorg Chem* 28:4411–4414
27. Wang J, Cheng C, Huang Y, Zheng B, Yuan H, Bo L, Zheng MW, Yang SY, Guo Y, Xiao D (2014) A facile large-scale microwave synthesis of highly fluorescent carbon dots from benzenediol isomers. *J Mater Chem C* 2:5028–5035
28. Liu DB, Chen WW, Wei JH, Li XB, Wang Z, Jiang XY (2012) A highly sensitive, dual-readout assay based on gold nanoparticles for organophosphorus and carbamate pesticides. *Anal Chem* 84:4185
29. Zhang RZ, Chen W (2014) Nitrogen-doped carbon quantum dots: facile synthesis and application as a “turn-off” fluorescent probe for detection of Hg^{2+} ions. *Biosens Bioelectron* 55:83–90
30. Dai HC, Shi Y, Wang YL, Sun YJ, Hu JT, Ni PJ, Li Z (2014) A carbon dot based biosensor for melamine detection by fluorescence resonance energy transfer. *Sensors Actuators B* 202:201–208
31. Wu HP, Huang CC, Cheng TL, Tseng WL (2008) Sodium hydroxide as pretreatment and fluorosurfactant-capped gold nanoparticles as sensor for the highly selective detection of cysteine. *Talanta* 76:347–352
32. Tang LB, Ji RB, Cao XK, Lin JY, Jiang HX, Li XM, Teng KS, Luk CM, Zeng SJ, Hao JH, Lau SP (2012) Deep ultraviolet photoluminescence of water-soluble self-passivated graphene quantum dots. *ACS Nano* 6:5102–5110
33. Chen X, Jin Q, Wu L, Tung C, Tang X (2014) Synthesis and unique photoluminescence properties of nitrogen-rich quantum dots and their applications. *Angew Chem Int Ed* 53:12542–12547
34. Cui X, Zhu L, Wu J, Hou Y, Wang P, Wang Z, Yang M (2015) A fluorescent biosensor based on carbon dots-labeled oligodeoxyribonucleotide and graphene oxide for mercury(II) detection. *Biosens Bioelectron* 63:506–512
35. Zhai X, Zhang P, Liu C, Bai T, Li W, Dai L, Liu W (2012) Highly luminescent carbon nanodots by microwave-assisted pyrolysis. *Chem Commun* 48:7955–7957
36. Zhang Y, Cui PP, Zhang F, Feng XT, Wang YL, Yang YZ, Liu XG (2016) Fluorescent probes for “off-on” highly sensitive detection of Hg^{2+} and L-cysteine based on nitrogen-doped carbon dots. *Talanta* 152:288–300
37. Zhang H, Huang Y, Hu S, Huang Q, Wei C, Zhang W, Kang L, Huang Z, Hao A (2015) Fluorescent probes for “off-on” sensitive and selective detection of mercury ions and L-cysteine based on graphitic carbon nitride nanosheets. *J Mater Chem C* 3:2093–2100
38. Liu HL, Wang YH, Shen AG, Zhou XD, Hu JM (2012) Highly selective and sensitive method for cysteine detection based on fluorescence resonance energy transfer between FAM-tagged ssDNA and graphene oxide. *Talanta* 93:330–335
39. Wei XY, Qi L, Tan JJ, Liu RG, Wang FY (2010) A colorimetric sensor for determination of cysteine by carboxymethyl cellulose-functionalized gold nanoparticles. *Anal Chim Acta* 671:80–84
40. Liu ZN, Zhang HC, Hou SF, Ma HY (2012) Highly sensitive and selective electrochemical detection of L-cysteine using nanoporous gold. *Microchim Acta* 177:427–433
41. Amini N, Shamsipur M, Gholivanda MB, Barati A (2017) A glassy carbon electrode modified with carbon quantum dots and polyalizarin yellow R dyes for enhanced electrocatalytic oxidation and nanomolar detection of L-cysteine. *Microchem J* 131:9–14
42. Xu XZ, Qiao J, Li N, Qi L, Zhang SF (2015) Fluorescent probe for turn-on sensing of L-cysteine by ensemble of AuNCs and polymer protected AuNPs. *Anal Chim Acta* 879:97–103
43. Shiu HY, Chong HC, Leung YC, Wong MK, Che CM (2010) A highly selective FRET-based fluorescent probe for detection of cysteine and homocysteine. *Chem-Eur J* 16:3308–3313
44. Shen YM, Zhang XY, Zhang YY, Zhang CX, Jin JL, Li HT, Yao SZ (2016) A novel colorimetric/fluorescence dual-channel sensor based on NBD for the rapid and highly sensitive detection of cysteine and homocysteine in living cells. *Anal Methods* 8:2420–2426